

ALMA Memo 422

The Dual-Load Calibration device revisited

S.Guilloteau (IRAM / ESO)

May 23, 2002

Abstract

Following ALMA memo 371, I re-investigate the dual load calibration scheme which has been proposed for ALMA. This memo improves on the requirements derived in memo 371 by using a better prediction for the atmospheric fluctuations at short time scales. It is shown that because of atmospheric properties and of the antenna geometry, a dual-load system located in the ALMA antenna subreflectors needs to switch at a rate in excess of 20–30 Hz to be efficient in the submillimeter regime. Moreover, integrations in excess of 10 seconds are required to get sufficient calibration accuracy at these frequencies. Because of the exceedingly high rate, and since the system has not been demonstrated to allow an absolute calibration, it is proposed to abandon this development.

1 Basic System Noise

The typical system temperature is derived from the agreed ALMA specifications, in the same way as in [Moreno & Guilloteau, memo 372]. I assume the standard ALMA numbers:

$$T_{\text{rec}}(\nu) = 6h\nu/k + 4 \text{ K} \quad (\nu < 400\text{GHz}) \quad \text{and} \quad T_{\text{rec}}(\nu) = 10h\nu/k + 4 \text{ K} \quad (\nu > 400\text{GHz})$$

for single sideband receivers (rejection better than 10 dB).

$$T_{\text{rec}}(\nu) = 3h\nu/k \text{ K} \quad (\nu < 400\text{GHz}) \quad \text{and} \quad T_{\text{rec}}(\nu) = 5h\nu/k \text{ K} \quad (\nu > 400\text{GHz})$$

for double sideband receivers. This ignores (for simplicity) more subtle dependence with frequency (specially for Band 7). I also assume the forward efficiency is falling down from 0.95 at low frequencies to 0.90 at 900 GHz (as ν^2).

The atmospheric conditions are taken from the weather statistics percentiles, with temperature adjusted to account (to first order) for the imperfect correlation between temperature and opacity. We assume dynamic scheduling will match the observed frequency to the appropriate observing conditions, more precisely that observations above 370 GHz will be done only in the 25 % best observing time, observations between 270 and 370 GHz only in the 50 % best observing time, and “low” frequency observations in the remaining available good weather (see Table 1). Figure 1 gives the corresponding expected system temperature **in the receiver calibration plane, i.e.**

$$T_{\text{ant}} = T_{\text{rec}} + J_{\text{sky}} \tag{1}$$

(see Eq.4 for the complete expression of J_{sky}). T_{ant} is the relevant quantity to compare with load temperatures (rather than the more usual system temperature outside the atmosphere, which is only relevant for the astronomical sources).

Percentile	$\tau(225 \text{ GHz})$	Water vapor		Temperature	Observing Frequency
		Max.	Typical		
75 %	0.117	< 2.3 mm	2.3 mm	+3°C	< 250 GHz
50 %	0.061	< 1.2 mm	1.0 mm	0°C	< 370 GHz
25 %	0.037	< 0.7 mm	0.5 mm	-5°C	700 GHz

Table 1: Adopted percentiles for the computation of the system temperatures. Note that this differs from individual percentiles by trying (grossly) to account for correlations between opacity and temperature.

2 Basic Equations

2.1 Standard Chopper / Vane Calibration

The calibration can be derived from the output powers measured by the receiver on the sky P_{sky} and when looking at a load P_{load} , compared to the correlated signal measured by the correlator, C_{source} :

$$\begin{aligned}
 P_{\text{sky}} &= K(T)(T_{\text{rec}} + J_{\text{sky}}) \\
 P_{\text{load}} &= K(T)(T_{\text{rec}} + fJ_{\text{load}} + (1 - f)J_{\text{sky}}) \\
 C_{\text{source}} &= K(T)g_s\eta e^{-\tau}T_A
 \end{aligned} \tag{2}$$

The coefficient $K(T)$ incorporates possible non linearity of the detector (receiver + amplifiers + backend). f is the fraction of the beam filled by the load, and η the forward efficiency. g_s and g_i are the normalized signal and image gain of the receivers $g_s + g_i = 1$. Note that, in terms of image to signal gain ratio, g ,

$$g_s = 1/(1 + g) \quad \text{and} \quad g_i = g/(1 + g) \tag{3}$$

The sky emissivity J_{sky} is given by

$$\begin{aligned}
 J_{\text{sky}} &= g_s(\eta J_{\text{m}}^s(1 - e^{-\tau_s}) + \eta J_{\text{bg}}^s e^{-\tau_s} + (1 - \eta)J_{\text{spill}}^s) \\
 &\quad + g_i(\eta J_{\text{m}}^i(1 - e^{-\tau_i}) + \eta J_{\text{bg}}^i e^{-\tau_i} + (1 - \eta)J_{\text{spill}}^i)
 \end{aligned} \tag{4}$$

where τ_j is the sky opacity (at the current elevation) and

$$J_{\text{x}}^j = \frac{h\nu_j}{k} \frac{1}{e^{h\nu_j/kT_{\text{x}}} - 1} \tag{5}$$

is the Rayleigh-Jeans equivalent temperature of a black body at T_{x} at frequency ν_j . j takes values s or i for signal or image bands respectively. J_{m} is the effective atmospheric brightness temperature, J_{bg} the cosmic background, and J_{spill} the spillover. Similarly, the effective load temperature J_{load} is

$$J_{\text{load}} = g_s J_{\text{load}}^s + g_i J_{\text{load}}^i \tag{6}$$

A major limitation of the calibration accuracy is the possible saturation of the receiver when looking at a warm load. Two strategies have been proposed to minimize this non linearity problem: the dual-load calibration in the subreflector [Bock et al. memo 225], or the semi-transparent vane [Plambeck memo 321]. A similar system was actually used on the IRAM Plateau de Bure antennas: the warm load could be inserted so as to cover partially the beam

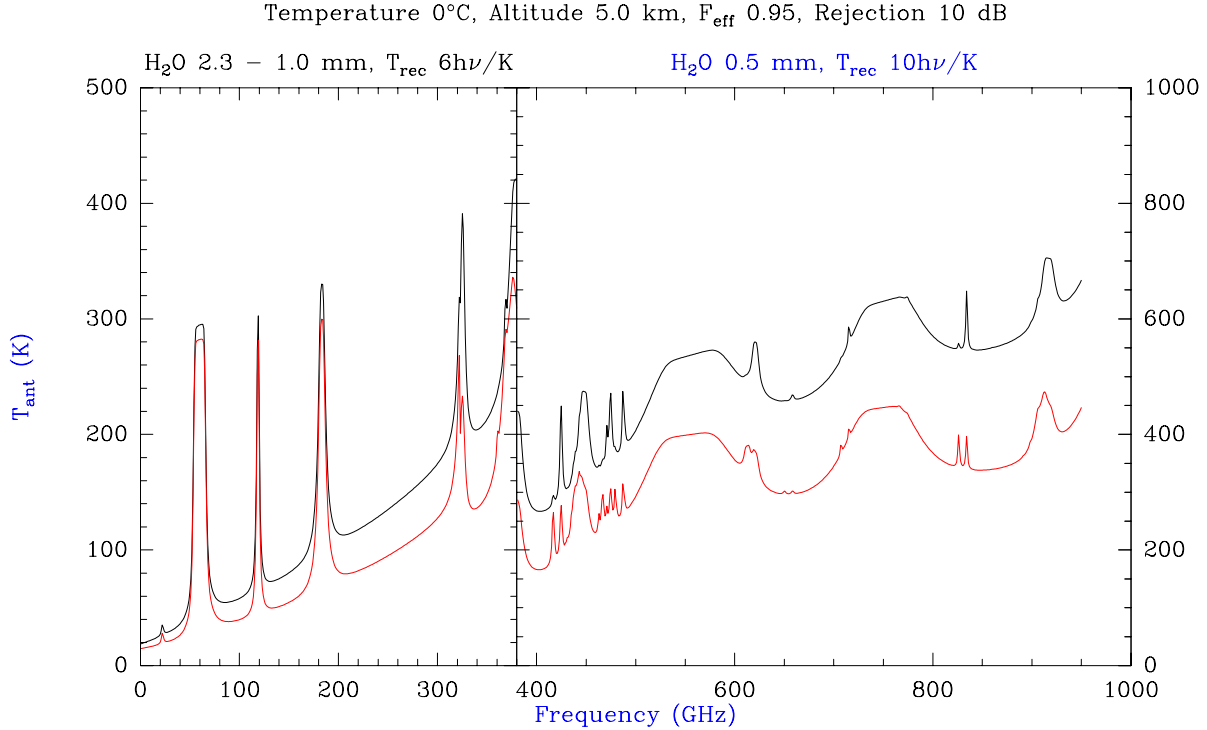


Figure 1: Expected typical antenna plane system temperatures with ALMA. The black curves correspond to Single Side Band tuned receivers (image rejection 10 dB), while the red curves correspond to Double Side Band tuned receivers. Created by `default_tant.astro`

of the receiver. This particular system was not extremely accurate because of the asymmetric blockage of the aperture. An homogeneous semi-transparent vane covering the whole beam is much preferable.

With a dual-load in the subreflector, the effective signal J_{load} can be small enough and comparable to the astronomical signal. For example, for ALMA antennas, a load could provide an effective temperature of about 0.6 K, which is a signal corresponding to a 18 Jy point source, i.e. comparable to that of the brightest quasars at mm wavelengths.

3 Subreflector dual-load system

Instead of having a load covering the full receiver beam, one can have a load in the subreflector which adds a weak signal to the power received from the sky. The output on such hot and cold loads is then

$$P_{\text{hot}} = K(T)(T_{\text{rec}} + fJ_{\text{hot}} + J_{\text{sky}} + g_s\eta e^{-\tau}T_A) \quad (7)$$

$$P_{\text{amb}} = K(T)(T_{\text{rec}} + fJ_{\text{amb}} + J_{\text{sky}} + g_s\eta e^{-\tau}T_A) \quad (8)$$

$$C_{\text{source}} = K(T)g_s\eta e^{-\tau}T_A \quad (9)$$

where f is a coupling coefficient between the load and the receiver. Eliminating the electronic gain $K(T)$.

$$K(T) = \frac{P_{\text{hot}} - P_{\text{amb}}}{f(J_{\text{hot}} - J_{\text{amb}})} \quad (10)$$

gives

$$T_A = \frac{e^\tau}{g_s \eta} f(J_{\text{hot}} - J_{\text{amb}}) \frac{C_{\text{source}}}{P_{\text{hot}} - P_{\text{amb}}} = T_{\text{cal}} \frac{C_{\text{source}}}{P_{\text{hot}} - P_{\text{amb}}} \quad (11)$$

The gain error is given by

$$\frac{\delta T_{\text{cal}}}{T_{\text{cal}}} = \frac{\delta T_{\text{load}} + \delta J_{\text{sky}}}{\Delta T_{\text{load}}} + 2 \frac{T_{\text{ant}}}{\Delta T_{\text{load}} \sqrt{\Delta \nu t}} \quad (12)$$

where $\Delta T_{\text{load}} = f(J_{\text{hot}} - J_{\text{amb}})$ is the apparent load temperature difference seen from the receiver, δT_{load} is the typical error on the true load temperature, δJ_{sky} the sky noise fluctuation during the measurement, and t the total time spent.

With the ALMA antennas, the coupling coefficient f to the loads in the subreflector can only be 0.8%, because of the small size of the subreflector and primary dish central hole. Thus, with the ‘‘hot’’ load at $T_{\text{hot}} = 100^\circ\text{C}$ and the load at ambient ($T_{\text{amb}} = 20^\circ\text{C}$), we have $\Delta T_{\text{load}} = 0.64$ K only. In the attempt to get **1 % absolute calibration**, I allocate a balanced error budget to these three terms

1. Effective load temperature difference 0.6 % $\Leftrightarrow \delta T_{\text{load}}/T_{\text{load}} = 0.006$
2. Noise term 0.6 % $\Leftrightarrow 2T_{\text{ant}}/\sqrt{\Delta \nu t} = 3.7$ mK
3. Sky stability 0.6 % $\Leftrightarrow \delta J_{\text{sky}} = 3.7$ mK

Point (1) has two contributions: the error on f and the errors (variations) on T_{hot} or T_{amb} . Equalizing these two terms requires to measure (or at least stabilize) the temperatures with 0.2°C accuracy, but also to determine the effective value of the coupling coefficient f to 0.41 % accuracy. This may prove extremely challenging.

The noise term (item 2) can be minimized at will, but it is important to keep in mind the typical values, since the minimum integration time is:

$$t > t_{\text{min}} = \frac{4}{\Delta \nu} \left(\frac{T_{\text{ant}}}{\sigma_a} \right)^2 = 0.36 (T_{\text{ant}}/100)^2 \quad (13)$$

for 8 GHz bandwidth (see Figure 2). While shorter than 1 second at frequencies below 300 GHz, this time rises up to 6-8 seconds at submm wavelengths.

The last problem in the sub-reflector load calibration is to avoid atmospheric fluctuations, which must remain below 3.7 mK. Sky fluctuations are given by

$$\delta J_{\text{sky}} = \sigma_A = \kappa(\nu) \sigma_w \min \left(\left(\frac{\Delta l}{300} \right)^q, \left(\frac{D}{300} \right)^q \frac{\Delta l}{D} \right) \text{ mK} \quad (14)$$

- $\kappa(\nu)$ is the ratio of water emission to pathlength fluctuations (in mK/ μm) at the observing frequency. κ is about 20 in the submm range (see Fig.3)
- σ_w is the atmospheric path rms fluctuations on a 300 m baseline
- Δl is the effective length over which the fluctuation occurs: for calibration, $\Delta l = vt/2$ where v is the tropospheric wind speed.
- the exponent q is the phase structure function exponent (0.6 on average).
- D is the antenna diameter (12 m).
- The min function derives from the fact that we have to consider two cases

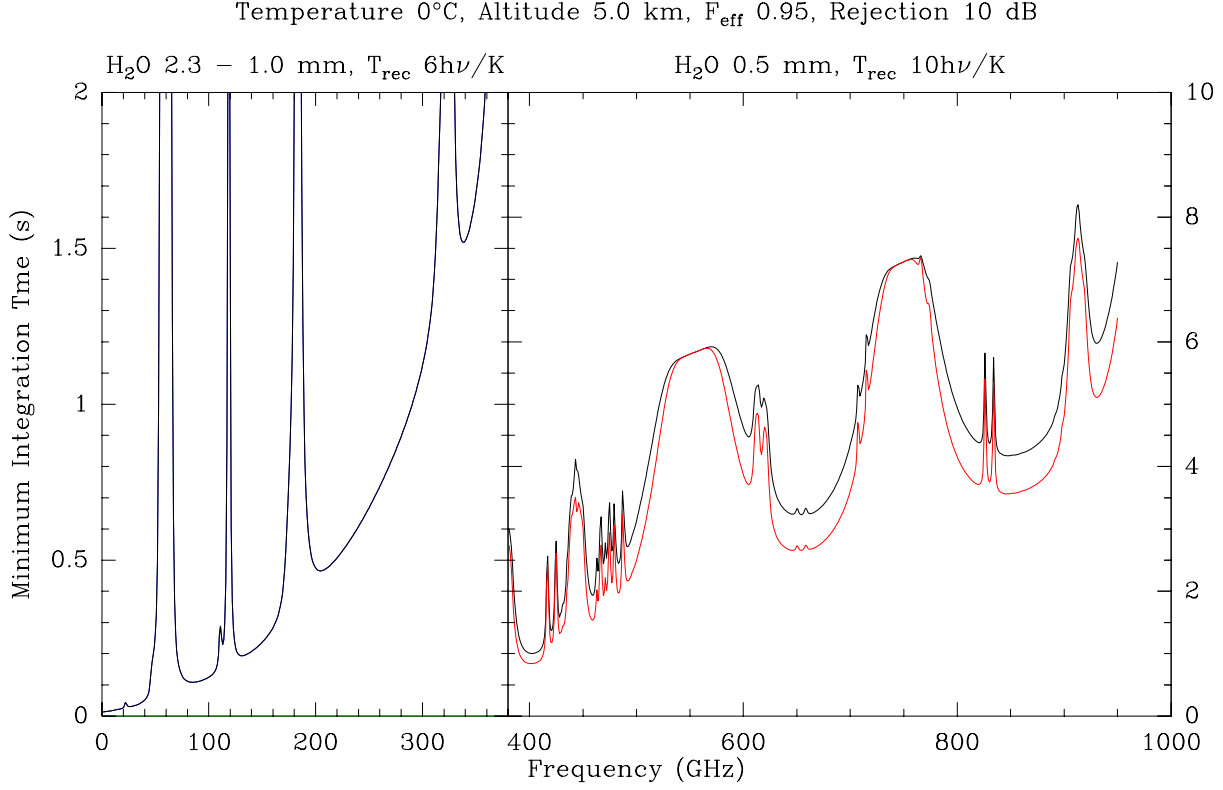


Figure 2: Minimum integration time for dual-load subreflector. The black curve is for typical conditions, the red curve is for optimal observing conditions (0.35 mm water vapor). Created by `default_i.astro`

1. The fluctuation time is longer than the crossing time of the atmosphere across the antenna diameter D . In the frozen atmosphere hypothesis, the two beams would then see patches separated by $\Delta l > D$, hence the fluctuation is given by the atmosphere structure function.
2. The fluctuation time is shorter than the crossing time. In this case, the two beams significantly overlap ($\Delta l < D$). The difference in the sky emission between the two beams is a finite difference of a smooth function (the antenna averaged sky emission), and hence scales linearly with Δl , with a proportionality factor equal to first derivative of the (antenna averaged) sky emission with distance.

The min function in Eq.14 derives from the continuity at $\Delta l = D$.

(The initial formula $\delta J_{\text{sky}} = \sigma_A = \kappa(\nu)\sigma_w \left(\frac{\Delta l}{300}\right)^{0.6} \frac{1}{\sqrt{1+(D/\Delta l)^2}}$ mK given in [Lucas memo 300] is incorrect).

$$\begin{aligned}
 \sigma_A &= \kappa(\nu)\sigma_w \left(\frac{vt}{600}\right)^q \text{ mK} \quad (t > 2D/v, \text{ or about } 2.5 \text{ s}) \\
 \sigma_A &= \kappa(\nu)\sigma_d \left(\frac{vt}{2D}\right) \text{ mK} \quad (t < 2D/v) \\
 \sigma_d &= \sigma_w(D/300)^q
 \end{aligned} \tag{15}$$

Using the median pathlength fluctuation, $\sigma_w = 250\mu\text{m}$ at 300 m, $q = 0.6$ and $D = 12$ m, we obtain $\sigma_d = 36\mu\text{m}$. With $v = 10$ m/s and $\kappa = 20$ as appropriate for the submm frequencies,

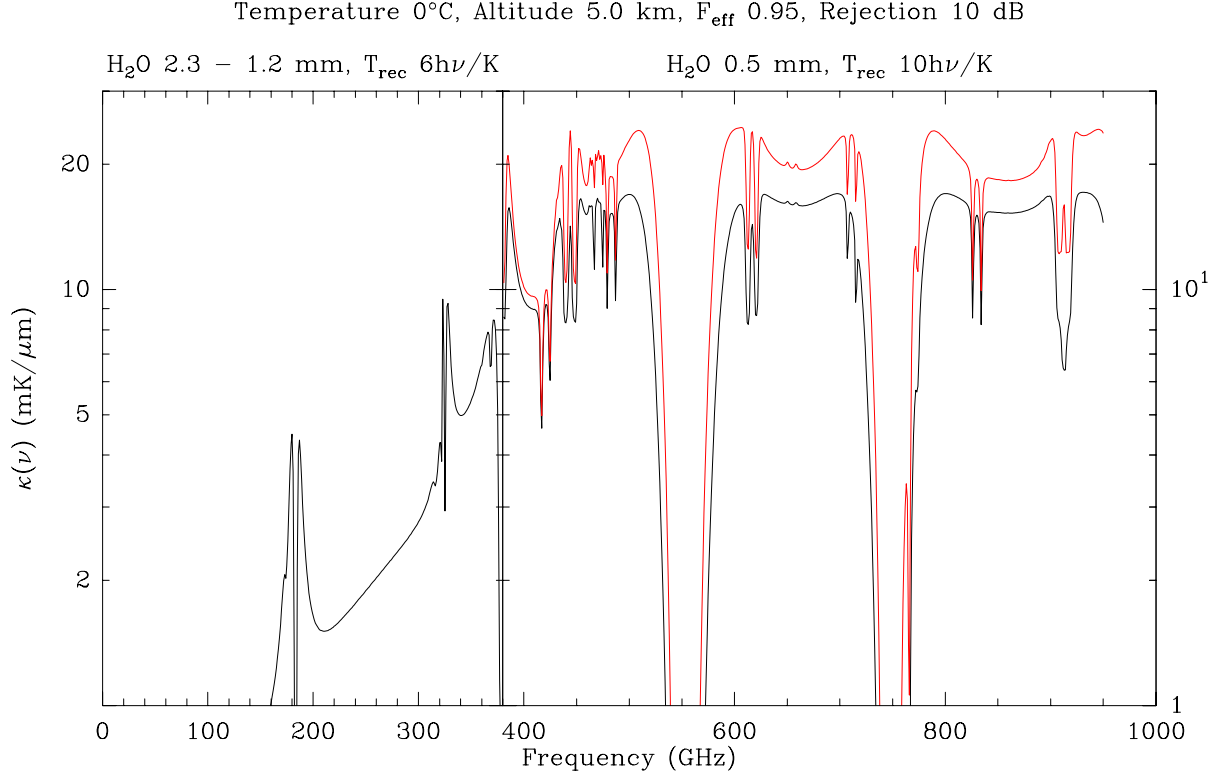


Figure 3: Relative sensitivity $\kappa(\nu)$ of sky emissivity to pathlength fluctuations. The black curve is for typical conditions, the red curve is for optimal observing conditions (0.35 mm water vapor). Created by `default_path.astro`

$\sigma_A \simeq 0.3$ K for a cycle time of 1 second. Hence, for $\kappa = 20$ (best transparency at submm wavelengths), we just obtain the required 3.7 mK fluctuation level for a 85 Hz switching period. It thus seems that such a calibration device should switch at very high frequency.

However, at such high switching rates, the radiometric noise dominates. In this case, we only need to balance the averaged noise contributions. In doing so, let us remember that n atmospheric fluctuations will not average as $1/\sqrt{n}$, since they are correlated. To account for this problem, I assume these n atmospheric fluctuations get averaged as n^{-s} , with s a free parameter: random fluctuations will have $s = 0.5$, but because of the atmospheric structure function $0 < s < 0.5$.

Calling p the switching cycle time, and t the total integration time, then $n = t/p$, and we want to equate the averaged atmospheric contribution $\sigma_A(p, t)$ with the radiometric noise $\sigma_r(t)$

$$\sigma_A(p, t) = \kappa(\nu)\sigma_d v / (2D)p(p/t)^s = 2 \frac{T_{\text{ant}}}{\sqrt{\Delta\nu t}} = \sigma_r(t) \quad (16)$$

For $s = 0.5$, we can eliminate t , and obtain

$$\kappa(\nu)\sigma_d v / (2D)p^{1.5} = 2 \frac{T_{\text{ant}}}{\sqrt{\Delta\nu}} \quad (17)$$

$$p = \left(\frac{DT_{\text{ant}}}{\kappa(\nu)\sigma_d v \sqrt{\Delta\nu}} \right)^{1/1.5} \quad (18)$$

Temperature 0°C, Altitude 5.0 km, F_{eff} 0.95, Rejection 10 dB

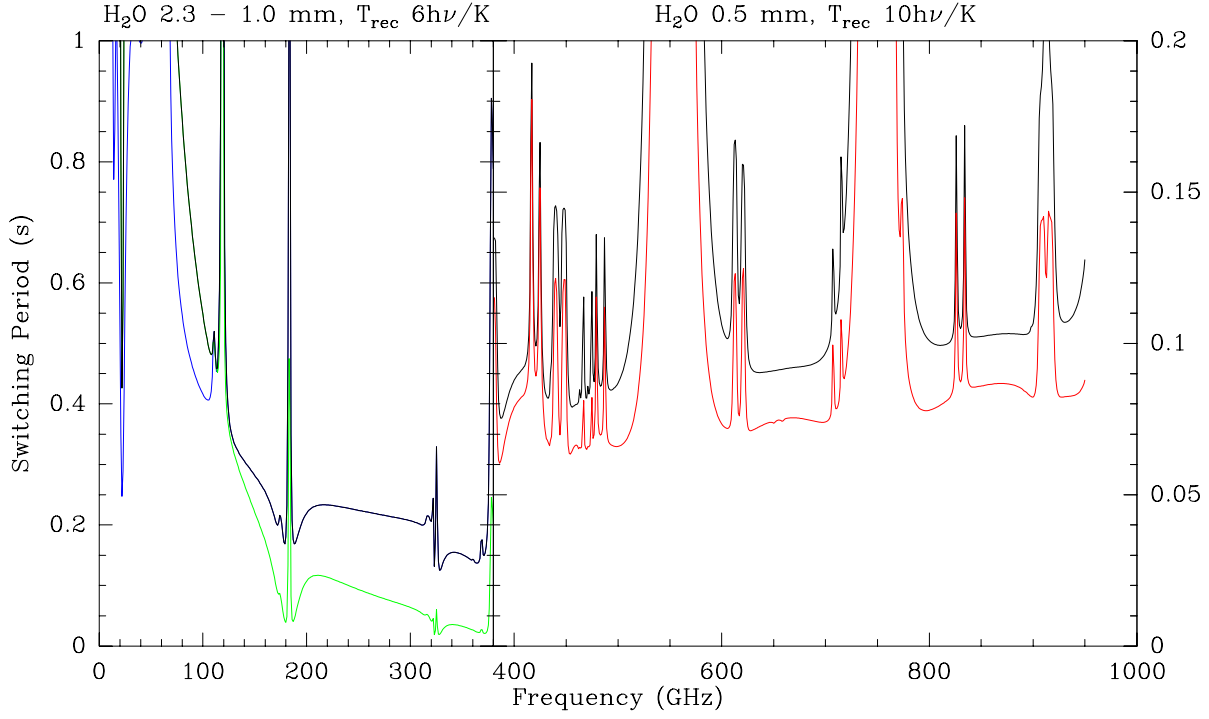


Figure 4: Maximum switching time for dual-load subreflector, assuming **uncorrelated** atmosphere. The black curve is for typical conditions, the red curve is for optimal observing conditions (0.35 mm water vapor). Below about 120 GHz, the switching time is limited only by the atmospheric noise $\sigma_A = 3.7$ mK (the blue curve would correspond to a limitation by thermal noise), while above 120 GHz, it becomes limited by the thermal noise also $\sigma_A = \sigma_r$ (the green curve would correspond by to a limitation by sky fluctuations only). Created by `default.p.astro`

This is given for $\Delta\nu = 8$ GHz in Fig.4, which indicates p is 0.07-0.1 seconds for nearly all frequencies above 400 GHz under typical conditions.

Unfortunately, the atmospheric fluctuations are correlated, so $s < 0.5$, and the period p depends on the integration time t .

$$p^{1+s} = t^{s-0.5} \frac{2D}{v\kappa(\nu)\sigma_d} \frac{2T_{\text{ant}}}{\sqrt{\Delta\nu}} \quad (19)$$

t must be sufficient to get the radiometric noise low enough; the **longest switching period** p_{max} is obtained using the minimal value t_{min} given in Eq.13:

$$p_{\text{max}} = \left(\frac{4}{\Delta\nu} \left(\frac{T_{\text{ant}}}{\sigma_A} \right)^2 \right)^{\frac{s}{1+s}} \left(\frac{\sigma_A 2D}{\sigma_d v} \right)^{\frac{1}{1+s}} \quad (20)$$

This is given for a few frequencies as a function of s in Fig.5. While values presented in Fig.4 are best cases, p_{max} can vary by as much as a factor 3–4 as a function of s .

This finding may look surprising since the prototype tests made at BIMA provide good results even with much longer periods [Bock et al. memo 225]. This has two origins. First, the BIMA device has been used only at 3 mm so far, in the regime longer than the crossing

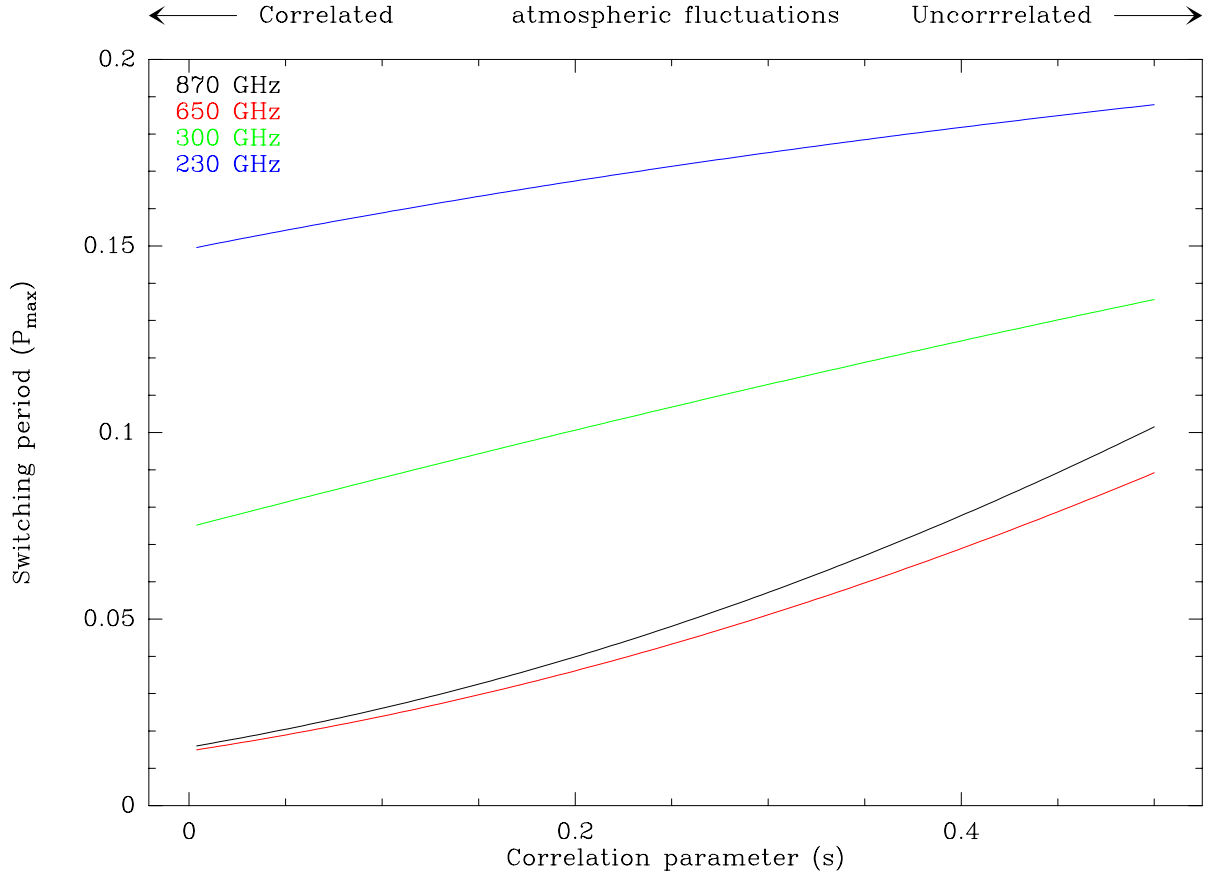


Figure 5: Maximum switching period p_{\max} for the dual-load subreflector as a function of atmospheric correlation for several frequencies. Created by `default_s.astro`

time of the atmosphere. Second, the coupling factor with the load is much larger at BIMA than for ALMA (2.2 % instead of 0.8 %). In this regime, the switching period p is given by

$$\kappa(\nu)\sigma_w \left(\frac{vp}{300} \right)^q = 0.7f\Delta T_{\text{load}} \quad (21)$$

$\kappa(\nu)$ is somewhat lower for BIMA than for ALMA, but σ_w probably larger (poorer site), so that the allowed period is 3-4 times longer for BIMA, of order several seconds for 90 GHz.

Note that in the other regime where sky noise and thermal noise have to be balanced, the dependencies of the switching period on site parameters is

$$p \propto \left(\frac{T_{\text{ant}}^2}{\Delta\nu} \right)^{\frac{s}{1+s}} f^{\frac{1-2s}{1+s}} \left(\frac{D}{\kappa(\nu)\sigma_d} \right)^{\frac{1}{1+s}} \quad (22)$$

As expected, in the $s = 0.5$ case (uncorrelated atmosphere), it depends only on the noise figure $T_{\text{ant}}^2/\Delta\nu$ and on atmospheric properties, but not on f . On the other hand, in the fully correlated case, $s = 0$, the period scales as $fD/(\kappa(\nu)\sigma_d)$ and does no longer depend on the noise. In practice, in the sub-mm domain, the problem is rather independent of the antenna and site parameters: the period must always be very short.

4 Discussion

The high switching rate required by the dual-load device, although not necessarily an unsolvable technical issue, has a number of implications on the overall system design. It requires a synchronous detection system to be useable. This makes it exceedingly difficult, if not impossible, to make calibrations with some spectral resolution, because that would require to synchronize the correlator acquisition with the load switching. This would be required only in auto-correlation mode, but that synchronization should apply to **all antennas** at once. Synchronization mechanical devices switching at 30 Hz over 64 antennas clearly represent a major task. It should be stressed that amplitude calibration with a spectral resolution of a few 10 MHz is required by ALMA, because of variations of the atmospheric transparency at such scale due to narrow lines of Ozone with significant opacity at sub-millimeter wavelengths.

While the above argument implies the system is not applicable to frequencies above 150 GHz or so, its applicability to lower frequencies is also questionable. A first problem concerns the level of standing waves which will be higher with the dual-load device than with an optimized sub-reflector with a conical inner part. This is specially important at low frequencies. A second, more fundamental, problem is the lack of absolute calibration: there is no way to measure (or predict) the exact coupling coefficient f except than to rely on a comparative measurement using an a-priori known calibrator. In such a process, one actually measures a product of f and of the antenna gain, which are difficult to separate but have different frequency dependence.

Table 2 summarizes the pro and cons of the dual-load system and the semi-transparent vane approach discussed in [Guilloteau & Moreno, memo 371] and [Guilloteau memo 423]. The vane approach clearly offers a number of advantages, in terms of speed, calibration, and maintenance facility. It is thus urgent to develop a prototype of the vane system

	Vane system	Dual-load
Location	In receiver cabin	<i>In subreflector</i>
Thermal control	At ambient, need measurement only	<i>Need heating system at 100°C in subreflector</i>
Speed	Slow device (1-2 sec)	<i>Fast switching (20-30 Hz)</i>
Reliability	Simple device	<i>Possible sealing problems at subreflector interface</i>
Maintenance	Easy access	<i>Awkward location</i>
Integration time	Short (< 1 sec)	<i>Up to 10 sec at submm frequencies</i>
Data Acquisition	Simple on 1 sec integration	<i>Requires demodulation scheme and synchronisation</i>
Basic Calibration	In a few minutes, on sky	<i>Not demonstrated</i>
Development	<i>to be done</i>	Prototype working
Standing Waves	minimal during observations	<i>Enhanced</i>
Spectral Resolution	Possible	<i>not possible</i>

Table 2: Pro and Con of the vane and dual-load calibration systems. **Pros** are in **boldface**, while *Cons* are in *italics*.

References

- [Lucas memo 300]
Lucas, R. (2000)
Reducing Atmospheric noise in single-dish observations with ALMA. *ALMA Memo 300*.
- [Plambeck memo 321]
Plambeck, R., 2000
Receiver Amplitude Calibration for ALMA *ALMA memo 321*
- [Bock et al. memo 225]
Bock, D., Welch, W.J., Fleming, M. & Thornton D., 1998
Radiometric Calibration at the Cassegrain Secondary Mirror. *ALMA memo 225*
- [Ulich & Haas, 1976]
Ulich, R. & Haas, R.W., 1976
Amplitude Calibration of Millimeter Wavelengths Spectral Lines. *ApJ Supp. 30, 247*
- [Moreno & Guilloteau, memo 372]
Moreno, R., & Guilloteau, S. 2002,
ALMA Calibration: Requirements on the integration times, and suggested observing strategies. *ALMA memo 372*
- [Guilloteau & Moreno, memo 371]
Moreno, R., & Guilloteau, S. 2001,
Receiver Calibration Schemes for ALMA. *ALMA memo 371*
- [Guilloteau memo 423]
Guilloteau, S. 2002,
The Vane Calibration System revisited. *ALMA memo 423*